Clemson University

TigerPrints

May 2020

Limb Bone Strains During Climbing in Green Iguanas: Testing Biomechanical Release as a Mechanism Promoting Morphological Transitions in Arboreal Vertebrates

Victor David Munteanu
Clemson University, munteanu.david@gmail.com

Follow this and additional works at: https://tigerprints.clemson.edu/all_theses

Recommended Citation

LIMB BONE STRAINS DURING CLIMBING IN GREEN IGUANAS:
TESTING BIOMECHANICAL RELEASE AS A MECHANISM PROMOTING
MORPHOLOGICAL TRANSITIONS IN ARBOREAL VERTEBRATES

A Thesis
Presented to
the Graduate School of
Clemson University

In Partial Fulfillment
of the Requirements for the Degree
Master of Science
Biological Sciences

---

by
Victor David Munteanu
May 2020

Accepted by:
Dr. Richard W. Blob, Committee Chair
Dr. Samantha A. Price
Dr. John D. DesJardins

ABSTRACT

Across vertebrate diversity, limb bone morphology is typically expected to reflect differences in the habitats and functional tasks with which species contend. Arboreal vertebrates are often recognized to have longer limbs than terrestrial relatives, a feature thought to help extend the reach of limbs across gaps between branches. Among terrestrial vertebrates, longer limbs can experience greater bending moments that might expose bones to a greater risk of failure. However, changes in habitat or behavior can impose changes in the forces that bones experience. If locomotion imposed lower loads in trees than on the ground, such a release from loading demands might have produced conditions under which potential constraints on the evolution of long limbs were removed, making it easier for them to evolve in arboreal species. We tested for such environmental differences in limb bone loading using the green iguana (*Iguana iguana*), a species that readily walks over ground and climbs trees. We implanted strain gauges on the humerus and femur, and then compared loads between treatments modeling substrate conditions of arboreal habitats. For hindlimbs, only surface angle indicated strain increases, whereas the forelimb lacked consistent evidence that treatments changed bone loading regimens directionally. In this system, biomechanical release seems to be an unlikely mechanism to have facilitated limb elongation; limb bone adaptations in arboreal habitats seem to be driven by selective pressures other than response to loading.

ACKNOWLEDGMENTS

TABLE OF CONTENTS

LIST OF TABLES

LIST OF FIGURES

I. INTRODUCTION

Many possible factors can contribute to the diversity in animal morphology (Gould and Lewinton 1979; Wainwright and Price 2016). Morphological diversity within vertebrate skeletons is often viewed as relating to differences in mechanical function (Wainwright et al. 2005; Aiello et al. 2017). One factor contributing to such views is the role of skeletons as load bearing structures (Turner 1998). Associations between bone shape and function are intuitive – changes in shape can impact the ability of a structure to bear loads (Lieberman et al. 2004; Rivera and Stayton 2011; McHenry et al. 2006), and changes in use have the potential to impact the loads to which a structure is exposed (e.g., Blob and Biewener 1999; Iriarte-Diaz 2002). For example, several studies have associated variation in limb bone morphology with differences in habitat and locomotor behaviors (Andersson 2004; Bergmann et al. 2009; Iriarte-Diaz 2002). However, measurements of how changes in habitat or behavior can impose changes in the forces to which bones are exposed are less common (Byron et al. 2011; Granatosky et al. 2018; Kemp et al. 2005; Young and Blob 2015).

One perspective that has emerged among studies that have examined changes in skeletal loading across changes in habitat or behavior is that such differences in loading might facilitate change in morphology. This can occur in cases of short-term acclimation of bone density in martial arts practitioners (Ito et al. 2016) and tennis players' dominant arms (Calbet et al. 1998), but can also extend into evolutionary timescales. For example, in comparisons of limb bone morphology between greyhounds (exposed to selection for running speed by humans) and pit bulls (exposed to selection for fighting prowess by humans), greyhounds showed gracile limb bones suited to produce long strides, whereas

pit pulls showed robust bones suited to resist high forces incurred during fighting (Kemp et al. 2005). Thus, particular structural features of limbs led to advantages in function that successfully passed through selection and contributed to changes in shape over the course of reproductive generations. However, an alternative perspective is that changes in environment may remove specific skeletal loading demands, and thus potentially open opportunities for morphological diversification. For example, among swimming turtles, the reduction of torsional strains during aquatic propulsion has been proposed to have removed specific advantages of tubular-shaped limb bones for resisting such loads – thus, greater opportunity for other shapes to evolve became possible, potentially enabling the eventual evolution of flattened limb bones among species that flap their limbs to swim, like sea turtles (Young and Blob 2015; Young et al. 2017). This specific novel morphological characteristic arose in a group reflecting transitions between terrestrial and aquatic habitats. Could changes in skeletal loading help to explain changes in limb shape across evolutionary transitions between other types of habitats?

Arboreal vertebrates have been described as having limb bones that are typically longer than those of closely related species that live mainly on the ground (Cartmill 1985; Kilbourne and Hoffman 2015; Rooney 2018; Herrel et al. 2013). Black-and-white ruffed lemurs (*Varecia variegata*) exemplify morphological changes that, when contrasted with more terrestrial taxa, would be advantageous for arboreal locomotor patterns (Meldrum et al. 1997). Although elongate limbs are considered advantageous during climbing to extend reach between grips, longer limbs also have greater moment arms for applied bending forces and would be expected to incur elevated bending loads during terrestrial locomotion (Biewener et al., 1983). The limbs of arboreal taxa are also known to have

2

significantly different loading patterns than those of terrestrial relatives (Demes et al. 2009; Lammers and Gauntner 2008). An arboreal species from which skeletal loads have been evaluated is the gibbon (*Hylobates lar*), in which recordings have been made from strain gauges implanted on the ulna, radius, and humerus during brachiation (Swartz et al. 1989). These data showed that the elongated limb bones of *H. lar* experienced high tensile (pulling or stretching) loads, which are unusual among vertebrate limb bones. Because brachiation is an unusual mode of locomotion among vertebrates, in which the body is suspended from the limbs rather than supported by them, it is unclear whether tensile loading might be expected among elongated limb bones of arboreal vertebrates more generally. However, it is also possible that, rather than elevation of specific types of loads promoting particular skeletal morphologies in arboreal taxa, a decrease in dominant loading regimes could open opportunities for a diversification of limb bone shapes (Young and Blob 2015). For example, animals climbing vertical surfaces might actually be pulled off of those surfaces by gravity (Maie et al. 2012), which could reduce the standard compressive or bending loads that such animals would experience during the support of body weight on level ground. Gravity might also pull climbing animals off of steep inclines, changing strain profiles in a similar fashion. Thus, either an increase in tensile loads or a reduction in compressive loads might contribute to conditions suitable for the evolution of bone elongation. In addition, compliance of arboreal substrates like branches might also reduce overall load magnitudes to which limb bones are exposed, such that elongated limb bones might not incur disadvantageous levels of bending and, therefore, have an increased potential to persist through the course of evolution, were they to appear.

This study tested for differences in limb bone loading during climbing compared to level locomotion, using bone strain measurements from the forelimbs and hindlimbs of green iguanas as a model. Through these measurements, I tested whether climbing produces patterns of skeletal loading consistent with expectations based on differences in limb morphology between arboreal and more terrestrial taxa, and whether biomechanical release from loading might have been a viable mechanism to have contributed to such changes.

II. MATERIALS AND METHODS

Animal collection and husbandry

Eleven *I. iguana* (SVL 28 – 37 cm) were collected from Palm Beach County, FL, USA using pole and noose, and were transported by car to our home lab facility in Clemson, SC, USA. Housing and husbandry followed published standards (Hatfield 1996) and Clemson IACUC requirements (AUP 2017-071 and 2018-041). Animals were housed in a greenhouse within large plastic enclosures (147L x 100W x 52H cm) fitted with climbing surfaces, basking areas, and hides to promote activity and enrichment. Temperatures were kept between 27 and 37°C with an ambient light:dark cycle and full spectrum lighting via direct sunlight provided by moveable panels in the greenhouse roof. Animals were supplied with water *ad libitum*, and were fed daily with a mix of collard greens, carrots, and mangoes, supplemented with a vitamin/mineral powder.

Surgical procedures

To conduct strain recordings, one rosette (FRA-1-11) and two single element (FLK-1-11) strain gauges (Tokyo Sokki Kenkyujo Co., Ltd., Japan) were surgically implanted onto the midshaft of each iguana's right femur or humerus, using aseptic technique. Techniques were based on procedures detailed in Blob and Biewener (1999). Anesthesia was induced by intramuscular injections of 60-100 mg/kg ketamine and 1 mg/kg xylazine into the left *M. triceps brachii* (Romer 1922), with analgesia provided through an injection of 1 mg/kg butorphanol at the same site. For animals with lower initial doses of ketamine, booster injections of up to 40mg/kg were given if a surgical plane of anesthesia was not achieved.

To implant the strain gauges, a longitudinal incision was made along the medial surface of the thigh or arm. For individuals in which femoral strains were measured, *M. iliotibialis, M. femorotibialis,* and *M. ambiens* were gently separated and retracted to expose the surface of the femur; for individuals in which humeral strains were measured, *M. biceps humerus* and *M. brachialis inferior* were separated and retracted to expose the humerus (Romer 1922). At sites selected for implantation, periosteum was removed by gentle scraping with a periosteal elevator, and the bone surface was swabbed clean with diethyl ether and allowed to dry for several seconds. Gauges were attached to the bone using self-catalyzing cyanoacrylate adhesive (Duro™ Superglue; Henkel Loctite Corp., Avon, OH, USA). Rosette gauges (FRA-1-11, Tokyo Sokki, Japan) were attached to the femur midshaft on the dorsal surface, and two single elements (FLK-1-11, Tokyo Sokki, Japan) were attached to the femur midshaft on the anterior and ventral surfaces, respectively. Gauges were attached to the humerus midshaft in a similar distribution, with the rosette placed on the anterior surface and two single elements placed in ventral and posteroventral positions. After the gauges were attached, lead wires (336 FTE, etched Teflon; Measurements Group, Raleigh, NC, USA) were passed subcutaneously to an incision made dorsal to the hip (femur) or the glenohumeral joint (humerus), where they exited the limb. Incisions were then sutured closed, and gauge wire contacts were soldered into a microconnector and secured with epoxy adhesive. Self-adhesive bandage was then wrapped around the exposed length of the lead wires to protect them and allow them to be secured as a cable to either the hip or shoulder region. Individuals were given 24 h to recover from surgery.

Strain data collection and analysis

The day following surgery, locomotor trials were conducted with each iguana in a wooden trackway (243L x 56W x 49H cm) with a clear Plexiglas panel on one side that allowed filming of trials. The trackway could be adjusted to simulate five environmental conditions, each of which was assigned an abbreviation as a naming convention: (1) a level trackway with a flat, non-compliant surface, simulating standard terrestrial substrates (FL-LEV); (2) a flat, non-compliant trackway angled at a 65° incline, simulating vertically inclined tree trunks common in arboreal habitats, particularly those growing over riverbanks common in the natural habitat of iguanas in Florida (FL-INC); (3) a level trackway with a compliant surface, formed by inserting a flexible (0.3 cm thick) plywood sheet into the trackway that could flex 7.5 cm at its midpoint between end supports that were 8.9 cm tall, simulating the compliance of branches found in many arboreal habitats (FL-COMP); (4) a level trackway with a curved surface, constructed from 30 cm diameter PVC pipe that was bisected longitudinally and laid along the length of the flat trackway, simulating the curvature of tree trunks (CRV-LEV); and (5) a trackway inclined at 65°, with the curved surface inserted (CRV-INC). For all trackway conditions, 0.7 cm-thick foam exercise mat was attached over all of the contact surfaces to improve grip of the iguanas' feet and limit slipping or sliding during locomotion. Trials across these different conditions allowed distinct consideration of the effects of different features of arboreal habitats on limb bone loading, including surface inclination, compliance, and geometry. Each animal was tested in each condition until ~20 step cycles were collected. However, the order of test conditions was randomized across animals.

To collect strain signals, the microconnectors were connected to Vishay conditioning bridge amplifiers (model 2120B; Measurements Group) via a shielded cable. Raw voltage signals were sampled through an A/D converter (PCI-6031E; National Instruments Corp., Austin, TX, USA) at 2500Hz, saved to computer using data acquisition code written in LabVIEW™ (v. 6.1, National Instruments) and calibrated to microstrain ($\mu\varepsilon$=strain x 10^{-6}). Trials were conducted to encourage a consistent speed for 1-4 step cycles. Although speeds may not have been strictly dynamically equivalent across different conditions (e.g. level versus inclined), they still provide data with comparable ecological relevance for understanding selection pressures on skeletal morphology. Strain trials were filmed from lateral perspective (120fps; GoPro Hero 3, GoPro, San Mateo, CA, USA). Video data were synchronized with strain recordings using a trigger connected to an LED visible in the camera frames that simultaneously produced 1.5 V pulses visible in strain records. Video frames marking the start and end of footfalls, as well as the time of the light pulse, were determined using Adobe Premiere Pro™ (Adobe, CC 2020 (14.0) / November 4, 2019). At the completion of all trials for an individual, each iguana was euthanized (Beuthanasia®-D pentobarbital sodium solution; Merck Animal Health, Millsboro, DE, USA; 200 mg/kg intraperitoneal injection) and frozen for later dissection of limb elements.

Conventions for the analysis and interpretation of strain data closely followed previous studies of skeletal loading in reptiles (Blob and Biewener 1999; Butcher et al. 2008; Sheffield et al. 2011). For each step, peak strain values for each axially aligned recording channel were extracted. In addition, magnitudes and orientations of peak principal strains (i.e. maximum and minimum strains at each site, regardless of alignment

with the femoral long axis), and shear strain magnitudes, were calculated from the output

of the three rosette gauge channels following published methods (Carter 1978; Dally and

Riley 1978; Biewener and Dial 1995). Values of principal strain orientations and shear

strain magnitudes provided insight into the importance of torsional loading: with the long

axis of each bone defined as 0°, pure torsional loads would show principal strain

orientations of 45° or -45°, depending on whether the bone was twisted in a clockwise or

counterclockwise direction. Data for the steps in each strain gauge metric for each

trackway condition (referred to as "cases") were compared using Mann-Whitney U-tests

conducted in R Statistical Software Version 3.6.1 (R Core Team, 2019).

III. RESULTS

In each animal, the implanted gauges allowed a potential for six strain magnitude cases to be compared across substrate conditions: one longitudinal strain magnitude value from each of the two single element gauges, and four strain magnitudes associated with the rosette gauge (longitudinal, principal tensile, principal compressive, and shear). The angle of principal tension to the long axis of the bone (ϕ_t) was also calculated for each step from rosette data, although these were not formally compared between conditions because this angle is included in the calculation of shear strains (Carter 1978; Biewener and Dial 1995), and it was deemed preferable to limit comparisons to variables directly related to strain magnitudes that could be connected to hypotheses about mechanisms of changes in bone shape. Representative strain traces for different substrate conditions are depicted for the femur in Figure 1, and for the humerus in Figure 2.

General patterns of limb bone strain in iguanas during locomotion

Strain patterns in the iguana femur for FL-LEV surfaces generally match those reported previously (Biewener and Blob 1999), although our new data include an additional recording location on the ventral aspect of the femur. Longitudinal strains increased as foot contact with the ground was made, reaching peak values near midstep, though there is some variability across recording locations and substrate types (Fig. 1). For three of the four iguanas from which we collected FL-LEV strains for the femur, strains were tensile on the dorsal surface, and compressive on the anterior surface (Table S1), reflecting loading of the femur in bending with a neutral axis running between these two gauge locations. These data resemble those collected by Blob and Biewener (1999)

specifically for the dorsal and anterior recording locations. Strains on the new, third, ventral location showed low levels of either tensile or compressive strain in the three iguanas with successful recordings, reflecting minor individual variation in loading across the animals. Principal strains for the dorsal recording location were considerably greater in magnitude than longitudinal strains, with magnitudes of ϕ_t averaging 49, 57, and 63° in the three iguanas with successful femoral rosette recordings. These values of near 45°, as well as shear strain magnitudes similar to those of principal strains, reflect the presence of torsional loading in the femur as well as bending during FL-LEV locomotion. Within each animal, strain patterns at a particular location typically were consistent across the different locomotor cases (e.g., gauges that showed tensile strains during FL-LEV also showed tensile strains in other loading conditions), though strain magnitudes sometimes differed (see below).

Strains in the iguana humerus for FL-LEV surfaces were similar among the individual iguanas, but show some differences from comparable humeral measurements reported previously in the American alligator, *Alligator mississippiensis* (Blob et al. 2014). Longitudinal strains increased as hand contact with the ground was made, reaching single maximum peak values near midstep, though there is some variability across recording locations and substrate types (Fig. 2). For three of the four iguanas from which we collected FL-LEV strains for the humerus, strains were tensile on the posteroventral and ventral surfaces. Both animals in which we were able to collect data from the anterior strain gauge indicated compressive strains on that surface (Table S1), reflecting loading of the humerus in bending with a neutral axis running between the ventral and anterior gauge locations. These specific data differ from patterns in *Alligator*

11

(Blob et al. 2014). Anteriorly placed gauges measured largely compressive strains in iguana humeri, whereas those measured in the alligator humerus were tensile. Similarly, ventrally placed gauges measured tensile strains in iguana humeri, and compressive strains in alligators. Strains on the new, third, posteroventral location showed similar tensile measurements as seen in the ventrally-located gauge. There is not a clear relationship between strain magnitude and gauge location. Principal strain orientations for the anterior recording location averaged ϕ_t of 47 and 53° in two iguanas, reflecting torsional loads superimposed on bending in the humerus during FL-LEV locomotion.

Strain magnitude comparisons across substrates

For the femur, the greatest directional effects of substrate type on strain magnitudes resulted from inclining the surface (Table 1). Twelve of 19 comparisons between FL-LEV and FL-INC substrates showed significant differences in strain, with 10 cases showing greater strains in inclined surfaces, and only two showing greater strains on level surfaces. However, seven of the 19 comparisons yielded no significant differences. Other comparisons across substrate types showed even fewer significant differences. Compliant substrates had little impact on the load magnitudes imposed on iguana femora, with 18 of 22 (82%) FL-LEV vs FL-COMP comparisons for the femur showing no significant differences. For cases that did show significant differences, three of four showed greater strains on compliant surfaces. Surface geometry, in comparisons of both level and inclined surfaces, also had little impact on load magnitudes. Fourteen of 19 comparisons (74%) between FL-LEV and CRV-LEV surfaces, and 23 of 28 comparisons (82%) between FL-INC and CRV-INC surfaces showed no significant differences. For cases that did show significant differences, the directionality of effects

12

was not consistent, with two of five cases showing greater strains on curved surfaces for level substrates, and one of five cases showing greater strains on curved surfaces for inclined substrates.

Surface inclination also showed the most frequent effects on loading for the humerus, though the directionality of effects was not as consistent as for the femur. Fourteen of 19 comparisons between FL-LEV and FL-INC substrates showed significant differences in strain for the humerus, but six cases showed greater strains on level surfaces, and eight cases showed greater strains on inclined surfaces. Similar to the femur, compliant substrates had little impact on load magnitudes for the iguana humerus, with four comparisons showing greater strains on compliant surfaces, but the remaining 15 of 19 (79%) comparisons showing no significant difference in strain between FL-LEV and FL-COMP surfaces. Surface geometry also had little impact on load magnitudes. Eleven of 17 comparisons (64%) for the forelimb between FL-LEV and CRV-LEV surfaces, and 11 of 19 comparisons (58%) between FL-INC and CRV-INC, showed no significant differences in strain. There was not a consistent pattern among cases that did show significant differences, with three of six showing greater strains on level curved surfaces, and 3 of eight showing greater strains on inclined curved surfaces.

Substrate Compared to Flat-Level Locomotion	Result of Comparison	Counts of Cases	
		Femur	Humerus
Flat-Incline	FL-LEV > FL-INC	2 (11%)	6 (32%)
	FL-INC > FL-LEV	10 (53%)	8 (42%)
	No signif. diff.	7 (36%)	5 (26%)
Compliant	FL-LEV > FL-COMP	1 (5%)	0 (0%)
	FL-COMP > FL-LEV	3 (14%)	4 (21%)
	No signif. diff.	18 (81%)	15 (79%)

Table 1 — Effects of substrate inclination and compliance on the absolute magnitudes of strains in iguana limb bones. Counts of cases that showed a particular comparison result are based upon all Mann-Whitney U-test comparisons (at $p < 0.05$), performed for each successfully recorded strain variable, within each individual iguana (see Tables S1, S2). Comparisons for other substrate conditions that were modeled did not yield significant or directional results.

Figure 1 (*following page*) — Femoral strain traces from representative limb cycles comparing flat (FL-LEV), incline (FL-INC), and compliant (FL-COMP) surfaces. Shaded regions indicate the time duration in which the pes is in contact with substrate.

FL-LEV   FL-INC   FL-COMP

ANTERIOR FEMUR (LONGITUDINAL)

VENTRAL FEMUR (LONGITUDINAL)

DORSAL FEMUR (LONGITUDINAL)

DORSAL FEMUR (PRINCIPAL - TENSION)

DORSAL FEMUR (PRINCIPAL - COMPRESSION)

DORSAL FEMUR (PHI)

DORSAL FEMUR (SHEAR)

15
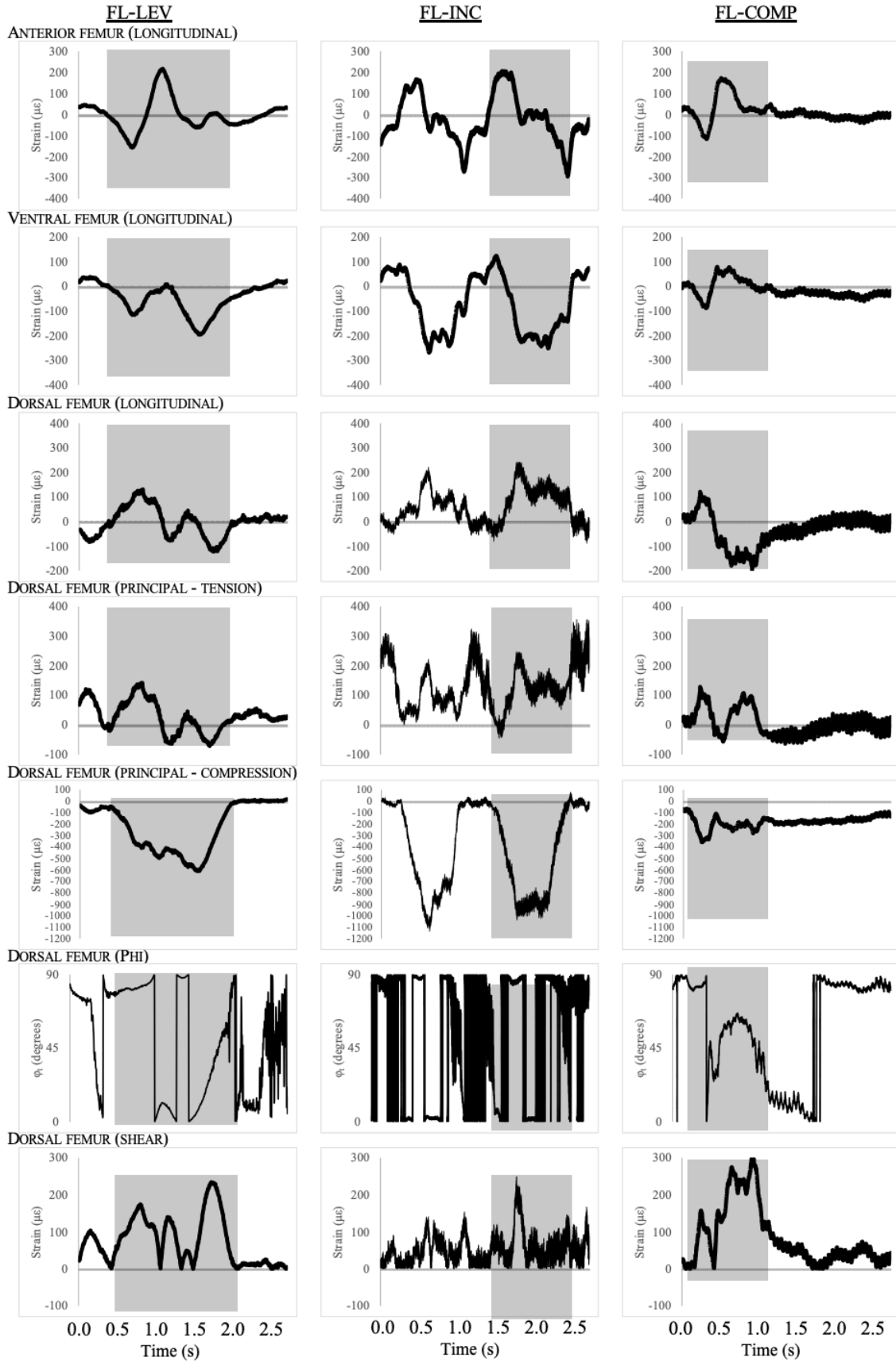
Figure 2 (*following page*) — Humeral strain traces from representative limb cycles comparing flat (FL-LEV), incline (FL-INC), and compliant (FL-COMP) surfaces. Shaded regions indicate the time duration in which the manus is in contact with substrate.

	FL-LEV	FL-INC	FL-COMP

POSTEROVENTRAL HUMERUS (LONGITUDINAL)

VENTRAL HUMERUS (LONGITUDINAL)

ANTERIOR HUMERUS (LONGITUDINAL)

ANTERIOR HUMERUS (PRINCIPAL - TENSION)

ANTERIOR HUMERUS (PRINCIPAL - COMPRESSION)

ANTERIOR HUMERUS (PHI)

ANTERIOR HUMERUS (SHEAR)

TIME (S)
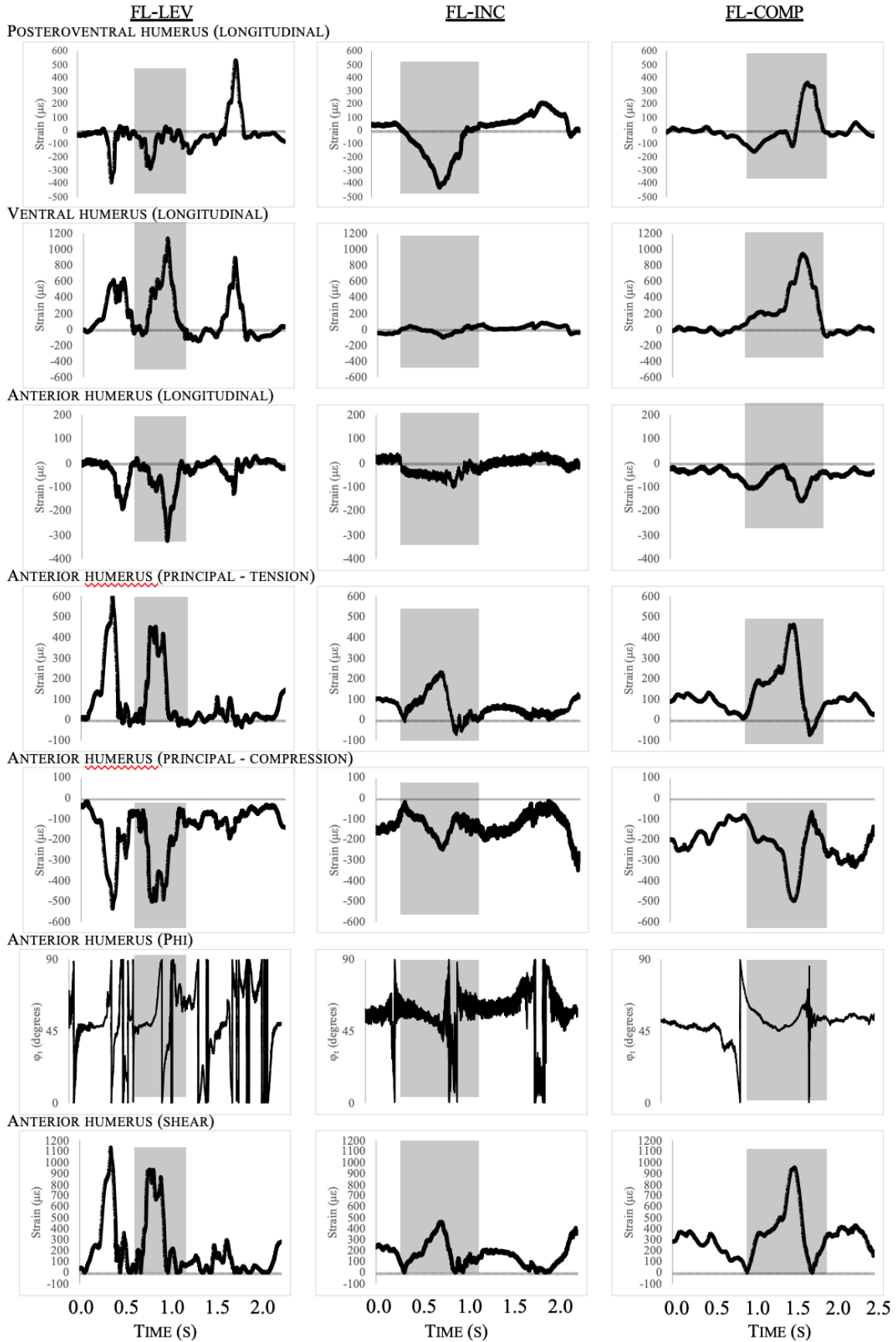
IV. DISCUSSION

Comparative limb bone loading mechanics during level locomotion

During locomotion on level, non-compliant surfaces, femoral strains recorded from the green iguana in this study were largely consistent with those recorded previously from this species (Blob and Biewener 1999), indicating substantial torsion superimposed on bending along an anterodorsal to posteroventral axis. Torsional loading of the femur appears to be a widespread feature of locomotion among tetrapods using sprawling locomotion (Butcher et al., 2008; Sheffield et al. 2011; Young et al. 2017), and potentially species using more upright posture as well (Carrano, 1998; Butcher et al., 2011; Copploe et al. 2015). In contrast to the similarities in femoral torsion across sprawling taxa, patterns of femoral bending are more diverse. The axis of bending in the iguana femur is similar to that in *Alligator* (Blob and Biewener 1999), running from anterodorsal to posteroventral; however, the dorsal aspect of the femur is loaded in compression in alligators, rather than in tension in iguanas. In contrast to these taxa, in both river cooter turtles (Butcher et al. 2008) and tegu lizards (Sheffield et al. 2011), the dorsal aspect of the femur is loaded in tension like in iguanas; however, the axis of bending in both of these species runs from anteroventral to posterodorsal. This diversity in femoral bending mechanics probably reflects a variety of kinematic differences across these taxa, particularly the extent to which the femur rotates about its long axis. Long axis rotation of limb bones changes the orientation of anatomical surfaces with respect to absolute space, such that largely vertical ground reaction forces (Kawano and Blob 2013) would place different anatomical surfaces of the femur in tension versus compression

18

about a bending axis that is horizontal in absolute space (Blob and Biewener 2001; Kawano et al. 2016). This possibility could be tested through the use of experimental techniques such as XROMM (X-ray Reconstruction of Moving Morphology: Brainerd et al. 2010), which can accurately and precisely resolve axial rotation of limb skeletal elements (Kambic et al., 2014; Mayerl et al., 2016).

Our recordings from the iguana humerus are the first humeral strains recorded from any lepidosaur. Strain patterns were different from those of the femur in some respects, despite both elements being proximal limb bones. For example, although torsion was prominent in the humerus as it was in the femur, the orientation of bending differed between these bones, placing the dorsal surface of the femur in tension in iguanas, but the ventral and posteroventral surfaces in tension in the humerus. Contrasts in loading between the femur and humerus were also observed in sprawling salamanders, and were interpreted as differences in the initial orientation and axial rotations of these elements through stance (Kawano et al. 2016). However, in addition to differences in axial rotation between these elements, it is also possible that the humerus and femur of iguanas differ in the magnitude of axial compression that is superimposed on their cross-sections in support of body weight. Increases and reductions of axial compression can shift the neutral axis of bending away from the cross-sectional centroids of bones, leading to changes in the distribution of tension and compression about the cortex (Blob and Biewener 1999). Because the iguana forelimb is smaller than the hindlimb, ground reaction force magnitudes or severity of effect may differ between the humerus and femur, contributing to differences in the distribution of their strains. Iguana humeral strains also differ from those of American alligators, which exhibit tensile strains on the

anterior and anteroventral surfaces, and compressive strains on the ventral surface.
Although the factors that contribute to the differences in axial compression between these
elements are unclear, they seem unlikely to relate to differences in axial compression
because the forelimbs are similar in proportion to the body in both taxa.

Environmental effects on limb bone loading and implications for biomechanical release

Out of all the simulated environmental conditions that we compared, only surface
incline had appreciable effects on limb bone loads during locomotion compared to level,
flat substrates – neither surface curvature nor compliance showed characteristic changes
in loading compared to level ground. These results indicate that, among the distinctive
components of arboreal habitats, the angle of the surface and the demands of climbing
vertically may place the greatest demands on the limbs. In the majority of the hindlimb
cases, the FL-INC (inclined) condition incurred significantly higher strains than those
incurred on the FL-LEV (level) condition. This directionality of effects was not as clear
for the humerus, but there were still several cases where the FL-INC condition incurred
significantly higher strains than FL-LEV, and average strain for the FL-INC was also
higher overall.

Data from this study were collected with the goal of gaining insight into how the
limbs of arboreal taxa lengthened through evolutionary time, particularly whether
lengthening of the limb bones might have been facilitated through opportunities provided
by a release from typical biomechanical loads during arboreal locomotion. Our results do
not support this conclusion. Rather than showing lower loads during simulations of
arboreal conditions, iguana limb bones did not show consistent changes in strains on
curved or compliant surfaces compared to flat, level ground. Only inclined substrates

20

showed prominent differences in loads from flat, level surfaces, but these more commonly showed higher, rather than lower strains. In this context, the evolution of longer limb bones in arboreal species may actually have occurred in spite of increases in overall strain, rather than being facilitated by a reduction in loads. Biomechanical release was likely an influential mechanism in other evolutionary habitat transitions, such as the secondary invasion of aquatic habitats by tetrapods (Young and Blob 2015; Young et al. 2017). However, it seems unlikely to have contributed to morphological changes across terrestrial-to-arboreal habitat transitions, suggesting that limb elongation in these transitions was driven by functional demands or other factors that superseded any potential costs of higher limb bone loads.

LITERATURE CITED

Aiello, B. R., Westneat, M. W., & Hale, M. E. (2017). Mechanosensation is evolutionarily tuned to locomotor mechanics. *Proceedings of the National Academy of Sciences 114*(17), 4459–4464.

Andersson, K. I. (2004). Elbow-joint morphology as a guide to forearm function and foraging behaviour in mammalian carnivores. *Zoological Journal of the Linnean Society* 142, 91–104.

Bergmann, P. J., Meyers, J. J., & Irschick, D. J. (2009). Directional evolution of stockiness coevolves with ecology and locomotion in lizards. *Evolution* 63, 215–227.

Biewener, A. A., Thomason, J., Goodship, A., & Lanyon, L. E. (1983). Bone stress in the horse forelimb during locomotion at different gaits: a comparison of two experimental methods. *Journal of Biomechanics 16*(8), 565–576.

Biewener, A. A., & Dial, K. P. (1995). In-vivo strain in the humerus of pigeons (*Columba livia*) during flight. *Journal of Morphology* 225, 61–75.

Blob, R. W., Espinoza, N. R., Butcher, M. T., Lee, A. H., D'Amico, A. R., Baig, F., & Sheffield, K. M. (2014). Diversity of limb-bone safety factors for locomotion in terrestrial vertebrates: evolution and mixed chains. *Integrative and Comparative Biology* 54:6, 1058–1071.

Blob, R. W., & Biewener, A. A. (1999). In vivo locomotor strain in the hindlimb bones of *Alligator mississippiensis* and *Iguana iguana*: implications for the evolution of limb bone safety factor and non-sprawling limb posture. *Journal of Experimental Biology* 202, 1023–1046.

Brainerd, E. L., Baier, D. B., Gatesy, S. M., Hedrick, T. L., Metzger, K. A., Gilbert, S. L., & Crisco, J. J. (2010). X-ray reconstruction of moving morphology (XROMM): precision, accuracy and applications in comparative biomechanics research. *Journal of Experimental Zoology Part A: Ecological Genetics and Physiology 313*(5), 262—279.

Butcher, M. T., Espinoza, N. R., Cirilo, S. R., & Blob, R. W. (2008). *In vivo* strains in the femur of river cooter turtles (*Pseudemys concinna*) during terrestrial locomotion: tests of force-platform models of loading mechanics. *Journal of Experimental Biology* 211, 2397–2407.

Butcher, M. T., White, B. J., Hudzik, N. B., Gosnell, W. C., Parrish, J. H., & Blob, R. W. (2011). In vivo strains in the femur of the Virginia opossum (*Didelphis virginiana*) during terrestrial locomotion: testing hypotheses of evolutionary shifts in mammalian bone loading and design. *Journal of Experimental Biology 214*(15), 2631–2640.

Byron, C., Kunz, H., Matuszek, H., Lewis, S., & Van Valkinburgh, D. (2011). Rudimentary pedal grasping in mice and implications for terminal branch arboreal quadrupedalism. *Journal of Morphology* 272, 230–240.

Calbet, J. A. L., Sanchis-Moysi, J., Dorado, C., Olmedillas, H., & Serrano-Sanchez, J. A. (2010). Bone and lean mass inter-arm asymmetries in young male tennis players depend on training frequency. *European Journal of Applied Physiology* 110, 83–90.

Carrano, M. T. (1998). Locomotion in non-avian dinosaurs: integrating data from hindlimb kinematics, in vivo strains, and bone morphology. *Paleobiology 24*(4), 450–469.

Carter, D. R. (1978). Anisotropic analysis of strain rosette information from cortical bone. *Journal of Biomechanics* 11(4), 199–202.

Cartmill, M. (1985). Climbing. In: Hildebrand, M. B., Liem, K. F., & Wake, D. M. (eds.): Functional Vertebrate Morphology. pp.73–88. Belknap Press, Cambridge, MA.

Copploe, J. V., Blob, R. W., Parrish, J. H., & Butcher, M. T. (2015). In vivo strains in the femur of the nine-banded armadillo (*Dasypus novemcinctus*). *Journal of morphology 276*(8), 889–899.

Dally, J. W., & Riley, W. F. (1991). Experimental stress analysis. New York: McGraw-Hill.

Demes, B., & Carlson, K. J. (2009). Locomotor variation and bending regimes of capuchin limb bones. *American Journal of Physical Anthropology: The Official Publication of the American Association of Physical Anthropologists*, *139*(4), 558–571.

Gould, S. J., & Lewontin, R. C. (1979). The spandrels of San Marco and the Panglossian paradigm: a critique of the adaptationist programme. *Proceedings of the Royal Society of London. Series B. Biological Sciences*, *205*(1161), 581–598.

Granatosky, M. C., Fitzsimons, A., Zeininger, A., & Schmitt, D. (2018). Mechanisms for the functional differentiation of the propulsive and braking roles of the forelimbs and hindlimbs during quadrupedal walking in primates and felines. *Journal of Experimental Biology* 221, jeb162917.

Hatfield, J. W. 1996. *Green Iguana: The Ultimate Owner's Manual.* Dunthorpe Press, Portland, OR.

Herrel, A., Tolley, K. A., Measey, G. J., da Silva, J. M., Potgieter, D. F., Boller, E., ... & Vanhooydonck, B. (2013). Slow but tenacious: an analysis of running and gripping performance in chameleons. *Journal of Experimental Biology*, *216*(6), 1025–1030.

Iriarte-Díaz, J. (2002). Differential scaling of locomotor performance in small and large terrestrial mammals. *Journal of Experimental Biology* 205, 2897–2908.

Ito, I. H., Mantovani, A. M., Agostinete, R. R., Junior, P. C., Zanuto, E. F., Christofaro, D. G. D., ... & Fernandes, R. A. (2016). Practice of martial arts and bone mineral density in adolescents of both sexes. *Revista Paulista de Pediatria* (English Edition), *34*(2), 210–215.

Kambic, R. E., Roberts, T. J., & Gatesy, S. M. (2014). Long-axis rotation: a missing degree of freedom in avian bipedal locomotion. *Journal of Experimental Biology 217*(15), 2770–2782.

Kawano, S. M., & Blob, R. W. (2013). Propulsive forces of mudskipper fins and salamander limbs during terrestrial locomotion: implications for the invasion of land. *Integrative and Comparative Biology 53*(2), 283–294.

Kawano, S. M., Economy, D. R., Kennedy, M. S., Dean, D., & Blob, R. W. (2016). Comparative limb bone loading in the humerus and femur of the tiger salamander: testing the 'mixed-chain' hypothesis for skeletal safety factors. *Journal of Experimental Biology 219*(3), 341–353.

Kemp, T. J., Bachus, K. N., Nairn, J. A., & Carrier, D. R. (2005). Functional trade-offs in the limb bones of dogs selected for running versus fighting. *Journal of Experimental Biology* 208, 3475–3482.

Kilbourne, B. M., & Hoffman, L. C. (2015). Energetic benefits and adaptations in mammalian limbs: scale effects and selective pressures. *Evolution* 69, 1546–1559.

Lammers, A. R., & Gauntner, T. (2008). Mechanics of torque generation during quadrupedal arboreal locomotion. *Journal of Biomechanics 41*(11), 2388–2395.

Lieberman, D. E., Polk, J. D., & Demes, B. (2004). Predicting long bone loading from cross-sectional geometry. *American Journal of Physical Anthropology* 123, 156–171.

Maie, T., Schoenfuss, H. L., & Blob, R. W. (2012). Performance and scaling of a novel locomotor structure: adhesive capacity of climbing gobiid fishes. *Journal of Experimental Biology 215*(22), 3925–3936.

Mayerl, C. J., Brainerd, E. L., & Blob, R. W. (2016). Pelvic girdle mobility of cryptodire and pleurodire turtles during walking and swimming. *Journal of Experimental Biology 219*(17), 2650–2658.

McHenry, C. R., Clausen, P. D., Daniel, W. J., Meers, M. B., & Pendharkar, A. (2006). Biomechanics of the rostrum in crocodilians: a comparative analysis using finite-element modeling. *The Anatomical Record Part A: Discoveries in Molecular, Cellular, and Evolutionary Biology: An Official Publication of the American Association of Anatomists 288*(8), 827–849.

Meldrum, D. J., Dagosto, M., & White, J. (1997). Hindlimb suspension and hind foot reversal in *Varecia variegata* and other arboreal mammals. *American Journal of Physical Anthropology: The Official Publication of the American Association of Physical Anthropologists 103*(1), 85–102.

Rivera, G., & Stayton, C. T. (2011). Finite element modeling of shell shape in the freshwater turtle *Pseudemys concinna* reveals a trade-off between mechanical strength and hydrodynamic efficiency. *Journal of Morphology 272*(10), 1192–1203.

Romer, A. S. (1922). The locomotor apparatus of certain primitive and mammal-like reptiles. *Bulletin of American Museum of Natural History 46*, 517–606.

Rooney, L. (2018). Postcranial Morphology and the Locomotor Adaptations of Extant and Extinct Crocodylomorphs and Lepidosaurs. East Tennessee State University Electronic Theses and Dissertations. Paper 3418.

Sheffield, K. M., M. T. Butcher, S. K. Shugart, J. C. Gander, R. W. Blob. (2011). Locomotor loading mechanics in the hindlimbs of tegu lizards (*Tupinambis merianae*): comparative and evolutionary implications. *Journal of Experimental Biology* 214, 2616–2630.

Swartz, S. M., Bertram, J., & Biewener, A. A. (1989). Telemetered in vivo strain analysis of locomotor mechanics of brachiating gibbons. *Nature* 342, 189–92.

Turner, C. H., & Pavalko, F. M. (1998). Mechanotransduction and functional response of the skeleton to physical stress: the mechanisms and mechanics of bone adaptation. *Journal of Orthopaedic Science* 3(6), 346–355.

Wainwright, P. C., Alfaro, M. E., Bolnick, D. I., & Hulsey, C. D. (2005). Many-to-one mapping of form to function: a general principle in organismal design? *Integrative and Comparative Biology* 45, 256–262.

Wainwright, P. C., & Price, S. A. (2016). The impact of organismal innovation on functional and ecological diversification. *Integrative and Comparative Biology* 56(3), 479–488.

Young, V. K. H., Wienands, C. E., Wilburn, B. P., & Blob, R. W. (2017). Humeral loads during swimming and walking in turtles: implications for morphological change during aquatic reinvasions. *Journal of Experimental Biology 220*(21), 3873–3877.

Young, V. K. H., & Blob, R. W. (2015). Limb bone loading in swimming turtles: changes in loading facilitate transitions from tubular to flipper-shaped limbs during aquatic invasions. *Biology Letters* 11, 20150110.

SUPPLEMENTAL MATERIALS

Table S1 (*pages 28–30*) — Hindlimb strain data across strain gauge metrics. "R" in gauge metric row indicates that this metric was associated with the rosette gauge. Values in first five rows indicate the average maximum/minimum strain (units in microstrain, $\mu\varepsilon$ = 10^{-6} × strain) ± standard deviation, with number of steps in parentheses. Bottom four rows indicate p-value of Mann-Whitney U-Tests comparing steps between two conditions. Bolding denotes significant differences between comparisons.

Gauge metric	IG01 SE-Ventral	SE-Anterior	SE-R Dorsal	R-pT	R-pC	R-Shear	R-Phi (units in degrees)	IG02 SE-Ventral	SE-Anterior	SE-R Dorsal	R-pT	R-pC	R-Shear	R-Phi (units in degrees)
FL-LEV	-164±156 (N=13)	-208±125 (N=13)	119±61 (N=13)	443±303 (N=13)	-416±259 (N=13)	278±155 (N=13)	49±26 (N=13)	133±76 (N=25)	-115±92 (N=25)	113±88 (N=25)	158±87 (N=25)	-435±417 (N=25)	260±186 (N=25)	63±40 (N=25)
FL-COMP	-78±57 (N=23)	-297±198 (N=23)	191±103 (N=23)	351±187 (N=23)	-600±380 (N=23)	281±142 (N=23)	45±27 (N=23)	172±119 (N=19)	-185±171 (N=19)	173±130 (N=19)	274±158 (N=19)	-797±490 (N=19)	378±123 (N=19)	53±25 (N=19)
FL-INC	-108±66 (N=13)	-758±239 (N=13)	570±189 (N=13)	576±187 (N=13)	-1680±509 (N=13)	489±104 (N=13)	22±20 (N=13)	161±97 (N=21)	-334±160 (N=19)	274±112 (N=21)	316±114 (N=21)	-1400±557 (N=18)	324±144 (N=21)	69±28 (N=21)
CURV-INC	-73±63 (N=13)	-336±304 (N=13)	426±344 (N=13)	475±291 (N=13)	-984±832 (N=11)	416±384 (N=13)	43±32 (N=13)	177±87 (N=19)	-236±122 (N=19)	276±121 (N=19)	325±124 (N=19)	-1090±493 (N=19)	376±144 (N=19)	76±12 (N=19)
CURV-LEV	-117±79 (N=8)	-117±98 (N=8)	108±80 (N=8)	417±180 (N=8)	-322±152 (N=8)	111±41 (N=8)	39±38 (N=8)	159±50 (N=22)	-106±87 (N=22)	143±110 (N=22)	600±566 (N=20)	-671±568 (N=22)	614±468 (N=20)	47±24 (N=20)
FL-COMP :: FL-LEV	0.123	0.100	**0.028**	0.397	0.065	1.000	0.626	0.335	**0.044**	0.187	**0.007**	**0.002**	**0.006**	1.000
FL-INC :: FL-LEV	0.687	**<0.001**	**<0.001**	0.091	**<0.001**	**<0.001**	**0.010**	0.123	**<0.001**	**<0.001**	**<0.001**	**<0.001**	**0.001**	**0.010**
CURV-LEV :: FL-LEV	0.750	0.140	0.336	0.750	0.301	**<0.001**	0.336	0.957	0.825	0.346	**<0.001**	0.118	0.153	0.314
CURV-INC :: FL-INC	0.169	**0.002**	0.204	0.223	**0.035**	0.153	0.072	0.892	0.893	0.728	0.113	0.247	0.226	

Animal	Gauge metric	IG03							IG04						
		SE-Ventral	SE-Anterior	SE-R Dorsal	R-pT	R-pC	R-Shear	R-Phi (units in degrees)	SE-Ventral	SE-Anterior	SE-R Dorsal	R-pT	R-pC	R-Shear	R-Phi (units in degrees)
	FL-LEV	78±91 (N = 27)	-258±219 (N = 24)	-197±83 (N = 27)	845±1 (N = 2)	-1543±331 (N = 7)									
	FL-COMP	114±131 (N = 32)	-251±148 (N = 32)	-132±78 (N = 32)											
	FL-INC	353±206 (N = 24)	-269±120 (N = 24)	-165±90 (N = 24)	313±177 (N = 24)	-802±429 (N = 24)	283±158 (N = 24)	48±25 (N = 24)	304±181 (N = 17)	285±322 (N = 16)	256±94 (N = 17)	354±650 (N = 17)	-768±238 (N = 17)	297±663 (N = 17)	16±13 (N = 17)
	CURV-INC	328±218 (N = 22)	-297±132 (N = 4)	-181±75 (N = 18)	281±207 (N = 17)	-630±368 (N = 17)	345±256 (N = 17)	31±21 (N = 17)	462±244 (N = 18)	125±49 (N = 15)	333±66 (N = 18)	487±287 (N = 18)	-809±264 (N = 18)	391±192 (N = 18)	18±18 (N = 18)
	CURV-LEV	114±204 (N = 12)	-190±144 (N = 12)	-209±99 (N = 12)	157±142 (N = 9)	-459±327 (N = 9)	139±140 (N = 9)								
	FL-COMP :: FL-LEV	0.071	0.503	**0.005**											
	FL-INC :: FL-LEV	**<0.001**	0.165	0.150	**0.006**	**<0.001**									
	CURV-LEV :: FL-LEV	0.749	0.271	0.685	**0.036**	**<0.001**									
	CURV-INC :: FL-INC	0.231	0.825	0.341	0.375	0.261	0.390		0.161	**0.011**	**0.013**	0.287	0.232	0.195	

Animal	Gauge metric	SE-Ventral	SE-Anterior	SE-Dorsal	R-pT	R-pC	R-Shear	R-Phi (units in degrees)
IG05	FL-LEV		-630±594 (N = 2)	268±38 (N = 2)	326±120 (N = 2)	-1392±376 (N = 2)	589±377 (N = 2)	57±38 (N = 2)
	FL-COMP		-529±220 (N = 15)	451±307 (N = 15)	531±281 (N = 15)	-1782±570 (N = 13)	563±248 (N = 15)	52±31 (N = 15)
	FL-INC							
	CURV-INC							
	CURV-LEV							
	FL-COMP :: FL-LEV		0.941	0.529	0.441	0.476	1.000	
	FL-INC :: FL-LEV							
	CURV-LEV :: FL-LEV							
	CURV-INC :: FL-LEV							
	CURV-INC :: FL-INC							

Table S2 (*pages 32–34*)— Forelimb strain data across strain gauge metrics. "R" in gauge metric row indicates that this metric was associated with the rosette gauge. Values in first five rows indicate the average maximum/minimum strain (units in microstrain, $\mu\varepsilon = 10{-}6 \times$ strain) ± standard deviation, with number of steps in parentheses. Bottom four rows indicate p-value of Mann-Whitney U-Tests comparing steps between two conditions. Boldface text denotes significant differences between comparisons.

Animal	Gauge metric	IG07							IG08						
		SE-Posteroventral	SE-Ventral	SE-R Anterior	R-pT	R-pC	R-Shear	R-Phi (units in degrees)	SE-Posteroventral	SE-Ventral	SE-R Anterior	R-pT	R-pC	R-Shear	R-Phi (units in degrees)
	FL-LEV	266±149 (N=23)	430±244 (N=23)						602±360 (N=23)	213±216 (N=23)	-169±114 (N=23)	434±176 (N=23)	-420±145 (N=23)	739±413 (N=23)	47±9 (N=23)
	FL-INC	241±113 (N=14)	478±200 (N=19)						531±448 (N=25)	157±174 (N=25)	-141±110 (N=25)	333±178 (N=25)	-386±137 (N=25)	683±309 (N=25)	49±4 (N=25)
	FL-COMP	430±143 (N=34)	833±274 (N=34)	-1338±262 (N=34)					178±118 (N=18)	139±82 (N=18)	-104±45 (N=18)	271±90 (N=18)	-297±65 (N=18)	528±167 (N=18)	50±4 (N=18)
	CURV-LEV								248±128 (N=26)	85±80 (N=26)	-132±58 (N=26)	374±140 (N=26)	-371±130 (N=26)	719±267 (N=26)	50±3 (N=26)
	CURV-INC	478±153 (N=16)	977±222 (N=16)	-1329±408 (N=16)											
	FL-COMP :: FL-LEV	0.654	0.341						0.436	0.356	0.346	0.087	0.449	0.413	
	FL-INC :: FL-LEV	**<0.001**	**<0.001**						**<0.001**	0.541	0.060	**0.001**	**0.004**	**0.025**	
	CURV-LEV :: FL-LEV								**<0.001**	**0.023**	0.480	0.315	0.220	0.571	
	CURV-INC :: FL-INC	0.180	0.057	0.827											

Animal	Gauge metric	IG09							IG12						
		SE-Posteroventral	SE-Ventral	SE-R Anterior	R-pT	R-pC	R-Shear	R-Phi (units in degrees)	SE-Posteroventral	SE-Ventral	SE-R Anterior	R-pT	R-pC	R-Shear	R-Phi (units in degrees)
IG09	FL-LEV														
	FL-COMP								-468±117 (N = 18)						
	FL-INC	178±154 (N = 23)		-329±116 (N = 23)	651±296 (N = 23)	-584±175 (N = 23)	983±318 (N = 23)	59±2 (N = 23)	-541±306 (N = 18)						
	CURV-INC	253±406 (N = 22)		-224±137 (N = 22)	413±87 (N = 22)	-446±93 (N = 22)	726±147 (N = 22)	59±4 (N = 22)	-336±434 (N = 2)						
	CURV-LEV								-504±121 (N = 17)						
	FL-COMP :: FL-LEV								0.053						
	FL-INC :: FL-LEV								0.046						
	FL-INC :: FL-LEV								0.012						
	CURV-LEV :: FL-LEV														
IG12	CURV-INC :: FL-INC	0.489		0.021	0.011	0.015	0.004		0.516						

Note: IG12 SE-Posteroventral also includes value -379±137 (N = 19).

Gauge metric	IG13 SE-Posteroventral	IG13 SE-Ventral	IG13 SE-R Anterior	IG13 R-pT	IG13 R-pC	IG13 R-Shear	IG13 R-Phi (units in degrees)	IG14 SE-Posteroventral	IG14 SE-Ventral	IG14 SE-R Anterior	IG14 R-pT	IG14 R-pC	IG14 R-Shear	IG14 R-Phi (units in degrees)
FL-LEV	304±115 (N = 18)	-166±73 (N = 18)		170±119 (N = 18)	-270±126 (N = 18)	227±87		358±179 (N = 17)	356±236 (N = 17)	-393±322 (N = 17)	773±316 (N = 17)	-939±415 (N = 17)	1593±851 (N = 17)	53±43 (N = 17)
FL-COMP	353±260 (N = 15)	-154±86 (N = 15)						537±212 (N = 15)	429±94 (N = 15)	-446±313 (N = 15)	987±330 (N = 15)	-1301±310 (N = 15)	2185±688 (N = 15)	47±7 (N = 15)
FL-INC	540±220 (N = 22)	-140±113 (N = 22)		196±89 (N = 22)	-317±132 (N = 22)	270±114 (N = 22)	36±16 (N = 22)	672±283 (N = 25)		-422±175 (N = 25)	1324±340 (N = 25)	-1430±381 (N = 25)	2648±699 (N = 25)	50±3 (N = 25)
CURV-INC	414±170 (N = 8)	-126±54 (N = 8)		146±67 (N = 8)	-278±152 (N = 8)	217±48 (N = 8)	44±18 (N = 8)	1040±386 (N = 22)		-414±176 (N = 22)	1712±457 (N = 22)	-1519±527 (N = 22)	2810±834 (N = 22)	51±5 (N = 22)
CURV-LEV	219±142 (N = 19)	-173±126 (N = 19)						259±273 (N = 17)	246±128 (N = 17)	-283±284 (N = 17)	1042±279 (N = 17)	-1167±337 (N = 17)	2166±594 (N = 17)	43±4 (N = 17)
FL-COMP :: FL-LEV	0.630	0.464						**0.014**	**0.009**	0.478	0.105	**0.007**	0.044	
FL-INC :: FL-LEV	**0.033**	0.400						**0.001**		0.185	**<0.001**	**<0.001**	**<0.001**	
CURV-LEV :: FL-LEV	**0.011**	0.918						0.140	0.058	0.114	**0.013**	0.057	**0.029**	
CURV-INC :: FL-INC	0.185	0.945		**0.002**	0.597	0.298		**<0.001**		0.941	**0.002**	0.466	0.547	